Title

Reaction of Iodine Atoms with Submicrometer Squalane and Squalene Droplets: Mechanistic Insights into Heterogeneous Reactions

Journal

The Journal of Physical Chemistry A, 118(45)

ISSN

1089-5639

Authors

Popolan-Vaida, Denisia M
Wilson, Kevin R
Leone, Stephen R

Publication Date

2014-11-13

DOI

10.1021/jp5085247

Peer reviewed

THE JOURNAL OF PHYSICAL CHEMISTRY A

Article

pubs.acs.org/JPCA

Reaction of Iodine Atoms with Submicrometer Squalane and Squalene Droplets: Mechanistic Insights into Heterogeneous Reactions

Denisia M. Popolan-Vaida,[†,‡] Kevin R. Wilson,[†] and Stephen R. Leone*[,†,‡,§]

[†]Chemical Sciences Division, Lawrence Berkeley National Laboratory, Berkeley, California 94720, United States

[‡]Department of Chemistry, University of California, Berkeley, California 94720, United States

[§]Department of Physics, University of California, Berkeley, California 94720, United States

ABSTRACT: The gas-phase reaction of iodine atoms with hydrocarbon molecules is energetically unfavorable, and there is no direct evidence for iodinated product formation by either H abstraction or I addition reactions at ambient temperature. Here we consider the possible heterogeneous reaction of I atoms with submicrometer droplets composed of a saturated alkane, squalane (Sq), and an unsaturated alkene, squalene (Sqe). The investigations are performed in an atmospheric pressure photochemical flow tube reactor in conjunction with a vacuum ultraviolet photoionization aerosol mass spectrometer and a scanning mobility particle sizer. Squalane, a branched alkane, is unreactive toward I atoms within the signal-to-noise, and an upper limit of the effective reactive uptake coefficient is estimated to be $\gamma_I^{Sq} \leq 8.58 \times 10^{-7}$. In contrast, the reaction of I atoms with unsaturated submicrometer squalene droplets results in observable iodinated squalene products. The effective reactive uptake coefficient of I atom with squalene particles is determined to be $\gamma_I^{Sqe} = (1.20 \pm 0.52) \times 10^{-4}$ at an average I concentration of 1.5×10^{14} molecules·cm^{-3}.

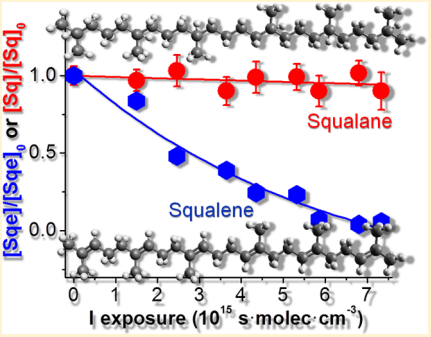

1. INTRODUCTION

Free radicals play key roles as initiators, propagators, or reactive intermediates of the complex chemical reactions involved in combustion, atmospheric chemistry, polymerization, plasma chemistry, biochemistry, and many other chemical processes.[1−5] Although several aspects of homogeneous gas and liquid phase chemistry of free radicals are quite well understood, there remains significant uncertainty about the heterogeneous reactivity of free radicals with organic surfaces composed of long chain hydrocarbons.

The hydrocarbon's free radical chemistry might considerably change with hydrocarbon phase (gas, liquid, or solid) or hydrocarbon degree of unsaturation (number of C═C bonds). The reactivity of organic particles is often considered within the context of known gas-phase reaction mechanisms in an effort to establish key similarities and differences between heterogeneous and homogeneous chemistry. However, rate coefficient predictions based upon gas phase structure−activity relationships cannot always be applied to heterogeneous reaction of free radicals with large hydrocarbons at the surface of a liquid droplet. Moise et al. showed that many types of chemical reactions that are slow in the gas phase are enhanced by several orders when they occur at an organic surface.[6]

Depending on the hydrocarbon degree of unsaturation the initial steps in hydrocarbon free radical chemistry might be H atom abstraction or free radical addition reactions. While the saturated hydrocarbon free radical reaction is initiated solely by the abstraction of a H atom by the radical species, the unsaturated hydrocarbon free radical reaction occurs either by H atom abstraction or by addition of radical species to the C═C double bond. These reactions result in the formation of alkyl radicals whose subsequent reactions are key steps in radical chain reactions in combustion chemistry, in the photochemical production of smog, or in heterogeneous aging of organic aerosols.

The halogens vary greatly in their reactivity toward hydrocarbons, considering a free radical initiation and possible chain reaction mechanism. In this context, it is of considerable interest to investigate the reactive behavior of I atoms, since iodine atoms and molecules are recognized to be the least reactive in the halogen activity series. For initiation, the I_2 molecule possesses intense absorption spectra in the visible, a region where few organic species absorb.[7,8] The simplicity of iodine photolysis in conjunction with I atom attack on specific organic sites makes photolysis of iodine in the presence of organic compounds a potential source of structurally specific R·, RO·, and RO_2· radicals. Because of their unique chemistry, I atoms are frequently used as an initiator in polymerization reactions.[9]

The gas-phase reaction of I atoms with a variety of alkanes[10−13] and alkenes[14−17] has been investigated experimentally as well as theoretically. While many aspects of the

Received: August 22, 2014
Revised: October 17, 2014
Published: October 20, 2014

homogeneous gas-phase chemistry of I atoms are well understood, little is known about the heterogeneous reactivity of I atoms with organic surfaces composed of long chain saturated and unsaturated hydrocarbons.

The reaction of squalane submicrometer particles with another halogen atom, Cl, has been investigated in this group in the absence and presence of oxygen.[18] In the absence of O_2, chlorinated reaction products are formed and an alkyl radical chain reaction propagates because of the presence of Cl_2. In the presence of O_2 (as much as 20%) the chain reaction is observed to effectively be shut off, as the Cl_2-propagated reaction instead produces oxygenated products.

The reactions of both squalane and squalene submicrometer particles with NO_3 have been studied as models for aerosol aging.[19] The reactive uptake coefficient measured for squalene was found to be about 2 orders of magnitude larger than the one measured for squalane. In addition, the reactive uptake measured for squalene increases with the squalene degree of oxidation from an initial value of 0.18 on fresh squalene aerosols to 0.82 for an average of more than three NO_3 reactions per squalene molecule in the aerosol.[19]

Recently, the kinetics and products of the heterogeneous OH-initiated oxidation of squalene submicrometer particles have been measured.[20] In the presence of as much as 10% O_2 in the flow reactor the effective uptake coefficient for squalene was found to be 2.34 ± 0.07, and the reactive uptake increases with $[O_2]$ in the reactor. The effective reactive uptake coefficient of squalene (which is dominated by secondary radical chain reactions) is also in this case about 1 order of magnitude larger than the one measured in the case of squalane under similar experimental conditions but only 5% O_2.[21]

Here the heterogeneous reaction of iodine atoms with submicrometer particles composed of squalane or squalene is investigated. These hydrocarbons represent simple model systems that can also successfully reproduce the reactive behavior of other molecules that are important chemical constituents of biofuel droplets or organic aerosols. The molecular structures of both squalane and squalene are shown in Figure 1.

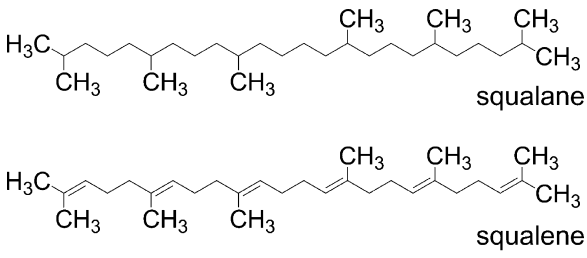

Figure 1. Chemical structures of the squalane and squalene molecules used in this study.

The heterogeneous reaction of I atoms with submicrometer squalane and squalene droplets is measured in a photochemical flow tube reactor with detection by a vacuum ultraviolet photoionization time-of-flight aerosol mass spectrometer (VUV-AMS). Aerosol mass spectrometry is used to measure heterogeneous reaction rates and product distributions in order to formulate a detailed reaction mechanism. The heterogeneous reactions of I atoms with submicrometer organic droplets composed of squalane or squalene are quantified to determine how the heterogeneous reaction rate of I atoms compares with previous measurements of Cl.

The main goal of the present studies is to evaluate simple model systems that are useful in developing a fundamental understanding of the mechanisms of heterogeneous reactions between small gas phase reactive species and submicrometer hydrocarbon particles. This paper also focuses on the reactive behavior of two molecules with similar structure but different reactivity due to the presence of C=C double bonds.

2. METHODOLOGY

2.1. Experimental Setup. The experimental setup employed in the present study, schematically presented in Figure 2, consists of an atmospheric pressure photochemical

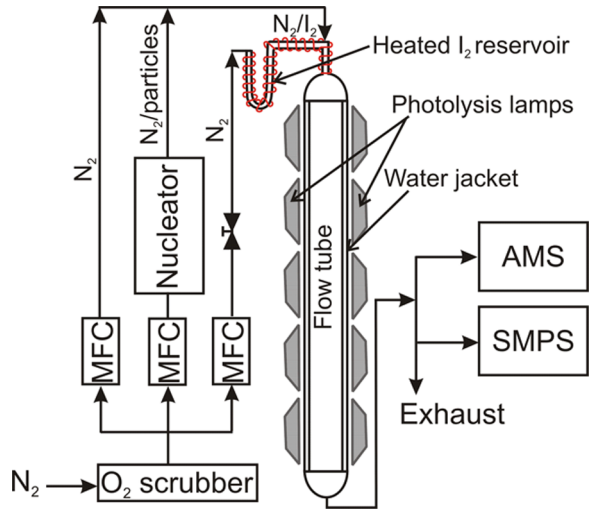

Figure 2. Schematic representation of the experimental setup employed to investigate the heterogeneous reactions between submicrometer droplets composed of squalane and squalene and I atoms. The total flow rate through the flow tube reactor is fixed to 1 slm over the duration of experiments which corresponds to a reaction time of 30 s. Iodine atoms are formed via the photolysis of I_2 by means of 10 halogen lamps. After reaction, the gas stream is sampled by a VUV-AMS and a SMPS to measure the particle composition and the particle size distribution, respectively.

flow tube reactor in conjunction with a scanning mobility particle sizer (SMPS) and an aerosol mass spectrometer (AMS). Details concerning the experimental technique are given elsewhere.[21] Briefly, submicrometer droplets of pure squalane and squalene are generated by homogeneous nucleation of the organic vapor in a 0.350 standard liter per minute (slm) flow of N_2 (high purity, 99.9999%) through a 45 cm long Pyrex tube containing the liquid samples. The Pyrex tube is heated in a tube furnace to 135 °C. Vapors of the organic compound become supersaturated upon leaving the heated region and nucleation occurs, yielding a log−normal particle size distribution with a geometric standard deviation of ~1.3 and a mean surface-weighted diameter of ~180 nm (mean surface-weighted diameter defines the average particle size based on the number distribution weighted by the surface area of the distribution). Gas phase I_2 vapor is generated by a flow of N_2 (high purity, 99.9999%) over iodine crystals (Sigma-Aldrich, ≥99.99%) placed in a 6 mm copper U-shaped tube located just before the flow tube reactor and surrounded by a heating tape, so the I_2 vapor pressure and consequently the I_2 concentration in the flow stream are maintained at a constant value for the duration of each experiment. I_2 is mixed with the particle

dx.doi.org/10.1021/jp5085247 | J. Phys. Chem. A 2014, 118, 10688−10698

stream in a balance of N_2 prior to entering the flow tube reactor. An O_2 scrubber (Sigma-Aldrich, 0.75 L Supelpure O trap) is placed in the N_2 lines to reduce the residual oxygen level to less than 0.5 ppm.

The mixed gases and particles are then introduced into a 100 cm long, 2.5 cm inner diameter Pyrex reaction cell, mounted vertically with the injection port at the top end. Iodine atoms are generated along the length of the reaction cell by I_2 photolysis using 10 continuous output halogen lamps, each 20 cm in length, placed in pairs along the length of the reactor. The atomic I concentration is controlled by adjusting the molecular iodine, I_2, concentration in the flow tube; i.e., the concentration of I_2 is increased by increasing the N_2 flow through the iodine cell at a constant I_2 cell temperature.

In order to prevent heating of the reaction flow due to the proximity of the halogen photolysis lamps, the flow tube is surrounded by a jacket through which thermostated water is circulated, enabling regulation of the reactor temperature. The reactor temperature was kept at 40 °C to prevent I_2 condensation on the reactor wall. The temperature of the flow tube is monitored using a K-type thermocouple and is essentially constant (<0.5 °C variation) over the duration of the experiment. The reactor and the surrounding halogen lamps are located in an opaque enclosure in order to prevent any I_2 dissociation due to ambient light.

Gas flows are regulated by calibrated mass flow controllers (MKS) before being transferred to the reaction system via copper tubing. The total flow rate through the flow tube was fixed to 1 slm, which, based on the illuminated section of the flow tube of 100 cm, corresponds to a reaction time of 30 s.

The chemical composition of the droplets is monitored using a custom built, soft-ionization aerosol mass spectrometer (VUV-AMS) as described by Gloaguen et al.[22] Briefly, a time-of-flight mass spectrometer is coupled to an aerodynamic lens for the purpose of focusing the particle beam and reducing the gas phase molecular concentration by means of pinhole plates described by Li et al.[23,24] The transmitted particles impinge on a heated copper block (~110 °C) where they are flash vaporized. The VUV-AMS measures droplet composition by thermally vaporizing the droplets followed by VUV photoionization of the gas phase species. Tunable VUV radiation is produced at the Chemical Dynamics Beamline of the Advanced Light Source. A part of the remaining flow exiting the reactor is sampled by a scanning mobility particle sizer (SMPS, TSI model 3936) to simultaneously determine the particle size distribution and number concentration.

2.2. Data Evaluation. To assess the experimental data, in particular, with respect to the reaction probability, the reaction models underlying the measured process are briefly outlined in this section. Details of the kinetic evaluation procedure are described elsewhere.[21]

The rate of a heterogeneous reaction with a gas phase reactive species is expressed as a reaction probability or reactive uptake coefficient (γ_X, where X = reactive species), which is defined as the fraction of collisions with a surface that results in a reaction. The uptake coefficient can be directly extracted by measuring the loss of a gas phase species exposed to a hydrocarbon surface. Often the gas phase reactive species are in very low concentrations and consequently very difficult or sometimes impossible to detect. An alternative approach to obtain an effective heterogeneous reaction probability (γ_X^{RH}) is to monitor the reaction via the condensed phase loss of the hydrocarbon (RH).

By use of a formalism developed by Smith et al.[21] for the reaction of OH radicals with squalane particles, the reaction probability for the reaction of an I atom with submicrometer hydrocarbon droplets RH (here RH = squalane or squalene) can be written as

$$\gamma_I^{RH} = \frac{4 \cdot k_{RH} \cdot D_{surf} \cdot \rho_0 \cdot N_A}{6 \cdot \bar{c} \cdot M_{RH}} \quad (1)$$

where k_{RH} represents a second order heterogeneous rate constant for the reaction of I atoms with the submicrometer hydrocarbon droplets, D_{surf} is the mean surface-weighted particle diameter, ρ_0 is the initial hydrocarbon molecule density (0.810 g·cm^{-3} for squalane and 0.858 g·cm^{-3} for squalene), N_A is Avogadro's number, $\bar{c}$ is the mean speed of gas phase I, and M_{RH} is the molar mass of the hydrocarbon molecule (422.81 g·mol^{-1} for squalane and 410.72 g·mol^{-1} for squalene).

From a plot of $[RH]/[RH]_0$ versus $\langle I \rangle_t t$ and fitting of the data to a first order exponential function, k_{RH} can be determined. $[RH]$ and $[RH]_0$ represent the final and the initial hydrocarbon concentrations, while $\langle I \rangle_t t$ is the average iodine atom exposure, obtained by multiplying the average iodine atom concentration $\langle I \rangle_t$ by the reaction time t.

A significant difficulty associated with the present study was the lack of a suitable choice of a reference gas phase reaction to obtain the I atom concentration. Instead, to quantify the concentration of gas-phase I atoms, the chemical kinetics program Kinetica2003 developed by Richardson et al.[25] is employed, together with the photolysis rate of I_2. Here, the program is used to model the time dependent I atom concentrations.

Because of the absence of appreciable side reactions of either I atoms or I_2 molecules with gas phase RH, or with O_2, H_2O, CO, or CO_2 that may be present in very small amounts in the reactor (as residual impurity in the N_2 carrier gas cylinder), the mechanism used to determine the I atom concentration in the flow tube consists of primarily three reactions (eqs 2a–2c).

$$I_2 + h\nu \xrightarrow{k_p} I + I \quad (2a)$$

$$I + I + N_2 \xrightarrow{k'} I_2 + N_2 \quad (2b)$$

$$I \xrightarrow{k''} \text{reactor walls} \quad (2c)$$

The first reaction considered is the photodissociation of the I_2 molecule (eq 2a). k_p denotes the I_2 photolysis rate constant, and its value is calculated as described in subsection 2.3. In addition to the photodissociation step, the I atom recombination (eq 2b) and I atom reaction with the reactor wall (eq 2c) are considered. k' represents the third order rate constant for the I atom recombination reaction and was set to a value of 1×10^{-32} cm^6·molecule^{-2}·s^{-1} (N_2 as collision partner, used in the present study) as reported by Jenkin et al.,[26] while k'' is a rate constant for I atom loss by reaction or recombination on the reactor wall. These three reactions primarily govern the I atom concentration in the flow tube reactor. The reaction and recombination of I atoms with the aerosol particles are not taken into account here because it accounts for less than 1% of the loss compared to the walls and the three-body recombination.

The loss of OH radical through reaction with the reactor wall was determined previously in this group by comparing the concentration of OH radical measured experimentally with that predicted from the concentration and photolysis rate of the OH

dx.doi.org/10.1021/jp5085247 | J. Phys. Chem. A 2014, 118, 10688–10698

precursor without the wall.[21] In this context, a value of 53 s^{-1} for the rate constant of the loss of OH at the reactor wall was determined. A similar value was obtained for the case of Cl atom wall loss.[18] Because of the poor reactivity of I atoms with tracer compounds, such as butane or hexanal, typically used in the experiments, the I atom wall loss rate could not be determined in a similar manner. Therefore, in the simulation k'' was set to a value of 53 s^{-1}, similar to that obtained for the OH wall loss. Possible errors that might result in determining the I atom concentration caused by the assumed k'' value are discussed in section 3.3.

In addition the program requires the input of the I_2 initial concentration and the concentration of the N_2 carrier gas. The concentration of I_2 is calculated from the N_2 flow rate through the iodine cell, regulated by means of a mass flow controller, and the I_2 vapor pressure at a certain temperature.

2.3. I_2 Rate of Photolysis. Ten halogen lamps (see section 2.1 for more details), which emit light between 380 and 1100 nm (as measured by an optical spectrometer, Ocean Optics HR4000), are used in the present experiment to produce atomic iodine via I_2 photodissociation.

The iodine molecule is known to absorb light in the visible region of the spectrum.[7,8] Two photodissociation channels can be accessed by means of visible light: (i) direct photodissociation via excitation of the A band, which leads to the formation of iodine atoms in the ground state, i.e., $I(^2P_{3/2})$, and (ii) indirect dissociation via excitation of the B state. The B-state is a bound state of I_2 and has a radiative lifetime on the order of microseconds.[27] However, the I_2 molecule when excited into the B-state can decompose to iodine atoms via collisional predissociation due to the coupling of the B-state with three repulsive states.[28] The predissociation rate of the B-state increases with the pressure, i.e., number of collisions.[27] Under our experimental conditions where the total pressure in the flow tube is ≥760 Torr, the relaxation of the excited I_2^* B-state molecule leads entirely to dissociation to I atoms ($I_2 + h\nu \rightarrow I_2^* + M \rightarrow I + I + M$).[29]

The rate at which I_2 is removed from the reaction cell as a result of photolysis can be calculated from the relation

$$k_p(\lambda) = \int_\lambda F(\lambda)\cdot\sigma(\lambda)\cdot\varphi(\lambda)\, d\lambda \quad (3)$$

where $F(\lambda)$ is the actinic flux (photons·cm^{-2}·s^{-1}·nm^{-1}), $\sigma(\lambda)$ represents the absorption cross-section (cm^2·$molecule^{-1}$) while $\varphi(t)$ is the quantum yield for photodissociation. The actinic flux can be determined from the relation

$$F(\lambda) = \frac{P}{S}\cdot\frac{1}{E} \quad (4)$$

where P is the power emitted by the photodissociation lamps, measured by a optical power meter (Coherent, FieldMate), S is the irradiated surface area, and E is the photon energy. In the present calculation of the actinic flux we considered only the photon flux that passes once through the reactor. We estimate that the light back-reflected by the opposite lamps (see Figure 2) has a contribution of less than 10% to the total light flux that illuminates the cell.

The value of the absorption cross-section over the wavelength range from 390 to 750 nm, reported with 1 nm resolution, is available from the literature.[30] $\varphi(\lambda)$ was set, for our calculations, at a value of 1 across the whole 390−750 nm spectrum.

Figure 3 displays the wavelength dependence of the I_2 photolysis rate, calculated at a resolution of 1 nm. Integration of the area under this plot gives a total $k_p(I_2) = 0.28 \pm 0.004$ s^{-1}.

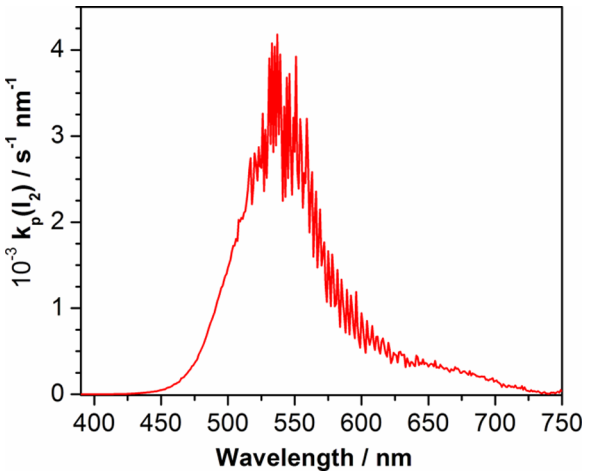

Figure 3. Wavelength dependence of the I_2 photolysis rate constant calculated at 1 nm resolution.

3. RESULTS AND DISCUSSION

The present investigations are designed in part to understand the pertinent difference between two organic systems with similar structure but different reactivity and mechanistic pathways as a result of carbon−carbon single bonds versus carbon−carbon double bonds. In this context, two sets of experiments were performed to investigate the heterogeneous reaction of saturated squalane and unsaturated squalene submicrometer hydrocarbon particles with I atoms.

As discussed above, the reactions of squalane and squalene submicrometer particles with I atoms are investigated in the photochemical flow tube reactor. In these experiments it is assumed that the reactant (squalane or squalene particles) is removed solely because of the reaction with iodine atoms. To verify this assumption, an initial set of experiments are performed to investigate the reaction of submicrometer droplets of squalane and squalene with molecular I_2 (photolysis lamps off). No evidence of product formation is observed to within the signal-to-noise of the photoionization mass spectrometer after the combination of I_2 alone with either squalane or squalene particles over the typical residence time (30 s) used in the present work, even after increasing the I_2 concentration to 5×10^{16} molecules·cm^{-3}. For experimental reasons, 5×10^{16} molecules·cm^{-3} was the highest I_2 concentration that could be achieved inside of the flow tube reaction for all experiments presented here. Furthermore, to test for the possible photolysis of the reactants with the lamps used in the present work, mixtures of the reactants (squalane or squalene particles) in nitrogen in the absence of iodine are irradiated; no photolysis of any of the reactants is observed.

3.1. Reaction of I Atoms with Squalane Submicrometer Droplets. Squalane ($C_{30}H_{62}$), a branched alkane, containing 8 primary, 16 secondary, and 6 tertiary carbon atoms, represents an ideal model system to mimic the variety of reactive carbon sites typically found on hydrocarbon surfaces and that may also occur in ambient organic aerosols. Abstraction is the only path available for the reaction of I

dx.doi.org/10.1021/jp5085247 | J. Phys. Chem. A 2014, 118, 10688−10698

atoms with alkanes. For this purpose the photoionization mass spectrum of unreacted squalane (no I_2 in the flow tube, photolysis lamps off) is recorded and compared to the photoionization mass spectrum of squalane reacted with I atoms for 30 s in the flow tube (I_2 in the flow tube, photolysis lamp on). No changes in the recorded product mass spectrum, compared to that of unreacted squalane, are observed by turning the halogen photolysis lamps on in the presence of I_2. The measurements were repeated several times at different I atom exposures by keeping the flow rate (i.e., reaction time) constant and varying the concentration of I atoms. No evidence for product formation is observed, even when increasing the concentration of I atoms in the flow tube up to 2.5×10^{14} molecules·cm^{-3}, by increasing the amount of I_2 precursor molecule up to 5×10^{16} molecules·cm^{-3}. For experimental reasons, 2.5×10^{14} molec·cm^{-3} was the highest I atom concentration that could be achieved inside the flow tube reactor. Under these experimental conditions, it appears that squalane submicrometer droplets react slower with I atoms than the experimental time scale allows.

On the basis of the background noise signal of the AMS (a maximum of 1 count per s) in the present experiment, peaks smaller than 0.02% of the unreacted squalane molecular ion intensity cannot be detected using the AMS technique. The absence of any type of reaction products in the reacted squalane mass spectrum indicates that either no products are formed or the amount of formed products is below the detection limit.

To consider the possibility of whether any alkyl radicals that are formed could be trapped chemically because of the reaction with an adjacent squalane molecule, i.e., by abstracting an H atom and re-forming squalane rather than reacting with an I atom or I_2 molecule, the reaction of squalane particles with iodine atoms was investigated in the presence of 20% O_2. If formed by an initial H atom abstraction by the I atom, an alkyl radical can react with O_2 to form peroxy radical. The peroxy radical self-reaction will then result in the production of higher molecular weight products with one oxygenated functional group. However, no evidence for oxygenated species is observed in the recorded mass spectra within the signal-to-noise ratio of the present experiment. This suggests that H abstraction followed by alkyl radical reactions is not occurring for the experimental conditions and with this signal-to-noise.

3.2. Reaction of I Atoms with Squalene Submicrometer Droplets. The reaction of squalene with I atoms is investigated using the same procedure as described for squalane particles. Squalene ($C_{30}H_{50}$) is an alkene that has 6 double bonds and 8 primary, 16 secondary, and 6 tertiary carbon atoms, making it an ideal proxy to represent the different kinds of reactive carbon sites typically found on hydrocarbon surfaces. In general, the course of reaction between an I atom and an alkene might include simultaneous contributions from addition, direct abstraction, and addition−elimination channels in contrast to the reaction of an I atom with alkane, where abstraction is the only path available. Addition is expected to be the major channel in the reactions of I atoms with squalene particles, which will proceed by I atom adding to one of the squalene double bonds and simple C−I bond formation. The formed adduct is an unstable radical and will further react. A second channel, consisting of direct abstraction of a hydrogen atom, might be also possible. The occurrence of this channel is more likely in the case of I atom reactions with alkenes than for the reactions with alkanes.[31] This can be explained by the lower value of the C−H bond dissociation energy for allylic hydrogen compared with that in alkanes and also by the possibility of an indirect addition−elimination process in the H atom abstraction.

Figure 4 displays the photoionization mass spectra of squalene particles (a) before and (b) after reaction with I atoms, recorded at a photon energy of 9.5 eV after evaporation of the reacted particles. A higher photon energy is observed to yield larger ion signals, but those photon energies also increase the fragmentation of the parent ions. Therefore, scans of multiple photon energies were performed (from 7.4 to 11 eV photon energy) and a compromise between overall signal strength and product fragmentation was made.

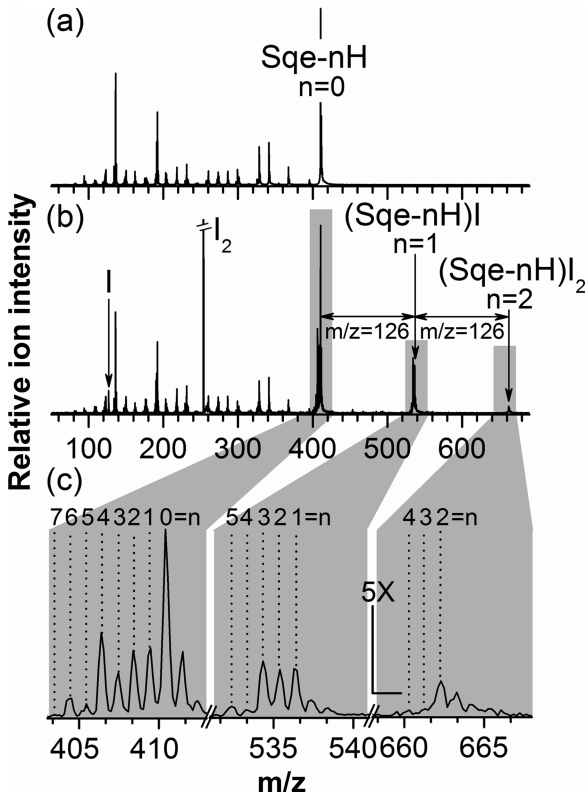

Figure 4. VUV-AMS mass spectra of squalene, measured at a photoionization energy of 9.5 eV, (a) before and (b) after exposure to I atoms ([I] = 2.445×10^{14} molecules·cm^{-3}). Panel c shows the product mass spectrum in panel b on a smaller scale that emphasizes the cluster of peaks at m/z = 403−413, m/z = 531−541, and m/z = 658−668, respectively.

Before the reaction (photolysis lamps off), the photoionization mass spectrum consists of a main peak located at m/z = 410 corresponding to the squalene molecular ion. No peaks with masses higher than squalene are observed in the absence of I atoms. Smaller peaks at masses lower than the mass of squalene are also observed, which correspond to squalene fragmentation due to dissociative photoionization or thermal dissociation (Figure 4a). When the photolysis lamps are turned on in the presence of I_2, the squalene peak decreases in intensity and the formation of reaction products is clearly observed (see Figure 4b). The reaction products appear in clusters of peaks separated by 126 amu. The first cluster of peaks is centered at m/z = 536, while the second cluster of peaks has the highest intensity peak located at m/z = 662. On the basis of the mass difference from the squalene molecular ion peak, the peaks located at m/z = 536 and 662 are consistent

dx.doi.org/10.1021/jp5085247 | J. Phys. Chem. A 2014, 118, 10688−10698

with products in which H atom(s) is(are) replaced by I atom(s) during the reaction. On the basis of the mass spectrum of reacted squalene particles shown in Figure 4b, no peaks are detected above the background signal at masses larger than m/z = 664.

There is neither evidence for products containing more than two I atoms nor products that involve polymerization after the I atom addition to the squalene molecule in the experiment. This indicates that within the signal-to-noise ratio of the present experiment either higher molecular weight products are not formed or they undergo dissociative photoionization during the ionization. Another explanation for the lack of higher molecular weight products (m/z > 664) in the squalene product mass spectrum might be due to their decomposition during the thermal vaporization of the aerosol prior to ionization. However, a closer look in the fragments region of the reacted squalene particle mass spectrum (Figure 4b) reveals that apart from three new peaks at m/z = 127, 128, and 254 corresponding to an I atom, HI molecule, and I_2 molecule, the mass spectrum remains essentially unchanged compared to the same region of unreacted squalene mass spectrum. The origin of atomic I and HI in the product mass spectra will be discussed later in this section. The I_2 molecule detected in the mass spectra can be explained by the recombination of the I atoms in the particle, because no I_2 signal is detected in the mass spectrum when the photolysis lamps are off (no I atoms are produced in the flow tube reactor). Therefore, we can rule out the possibility that I_2 signal observed in the product mass spectrum originates from I_2 dissolved into the hydrocarbon particle and subsequently liberated from the particle during the vaporization on the copper block. Consequently, the observed reaction is exclusively initiated by the I atoms formed in the gas-phase.

Finally, the formation of polymerized products cannot be excluded. It might be possible that such products are formed, but they are not effectively detected because of the fact that their volatility might be much lower than the squalene volatility. As mentioned above, the temperature of the copper block was kept at 110 °C in our experiments to preserve the squalene molecular ions.

Apart from the iodinated products, several peaks at masses slightly lower than the mass of squalene, such as m/z = 409, 408, etc., are also observed (see Figure 4c, left panel). These peaks correspond to dehydrogenated squalene. As can be seen in Figure 4c middle and right panels, dehydrogenated iodinated products are also observed. The possible origin of these peaks is discussed later in this section.

Figure 5 displays the 402−416 amu region of the squalene mass spectra recorded before (Figure 5a) and after (Figure 5b−f) exposure to different amounts of I atoms. No dehydrogenated squalene is observed when no I atoms are present in the flow tube (Figure 5a). When the concentration of atomic I in the flow tube reactor is gradually increased from approximately 5.01 × 10^{13} molecules·cm^{-3} (Figure 5b) to 2.45 × 10^{14} molecules·cm^{-3} (Figure 5g), the sequential formation of Sqe-H, Sqe-2H, etc. is observed. The distribution of the dehydrogenated squalene products appears to be correlated with the I atom concentration in the flow tube.

One possible explanation for the formation of dehydrogenated squalene peaks might be attributed to intermolecular H abstraction by the iodinated products. The alkyl radical formed after I addition might participate in further abstraction reactions in the particle and abstract a H atom from an adjacent squalene

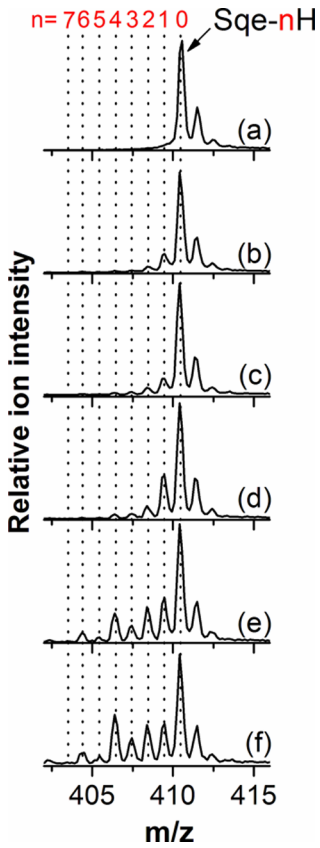

Figure 5. The 402−416 amu region of the squalene mass spectra recorded (a) before and (b−f) after the exposure to different amounts of I atoms. The concentration of I atoms in the flow tube is (b) 5.007 × 10^{13} molecules·cm^{-3}, (c) 8.212 × 10^{13} molecules·cm^{-3}, (d) 1.450 × 10^{14} molecules·cm^{-3}, (e) 1.951 × 10^{14} molecules·cm^{-3}, and (f) 2.445 × 10^{14} molecules·cm^{-3}.

molecule or its products, resulting in the formation of allylic Sqe-nH and (Sqe-nH)I products. When O_2 is present, the allylic radicals can react with O_2 and form peroxy radicals. Therefore, the squalene + I reaction is investigated in the presence of oxygen (not shown here). In the presence of as much as 20% O_2 in the flow tube reactor during the reaction, the intensity of the dehydrogenated squalene and iodinated squalene dehydrogenated peaks considerably decreased. Instead, new clusters of peaks separated by m/z = 16 are observed in the recorded mass spectrum. The new peaks corresponding to the formation of oxygenated reaction products are consistent with molecules containing alcohol and ketone functional groups. In addition, there is also a clear evidence for a significant number of reaction products that contain a mixture of oxygen and iodine atoms. The formation of oxygenated peaks, correlated with the decrease of the dehydrogenated peaks when oxygen is present in the reactor, indicates the occurrence of allylic chemistry.

The Sqe-nH and (Sqe-nH)I_n peaks might also partially be attributed to dissociative photoionization of higher molecular weight products as discussed later in this section. However, understanding the formation chemistry of these dehydrogenated peaks is beyond the scope of this publication.

Furthermore, peaks with mass slightly higher than squalene, i.e., m/z = 411, 412, and its iodinated products, i.e., m/z =537, 538, 663, 664, are also observed. The nature of these peaks can be explained by the natural isotopic abundance of carbon

dx.doi.org/10.1021/jp5085247 | J. Phys. Chem. A 2014, 118, 10688−10698

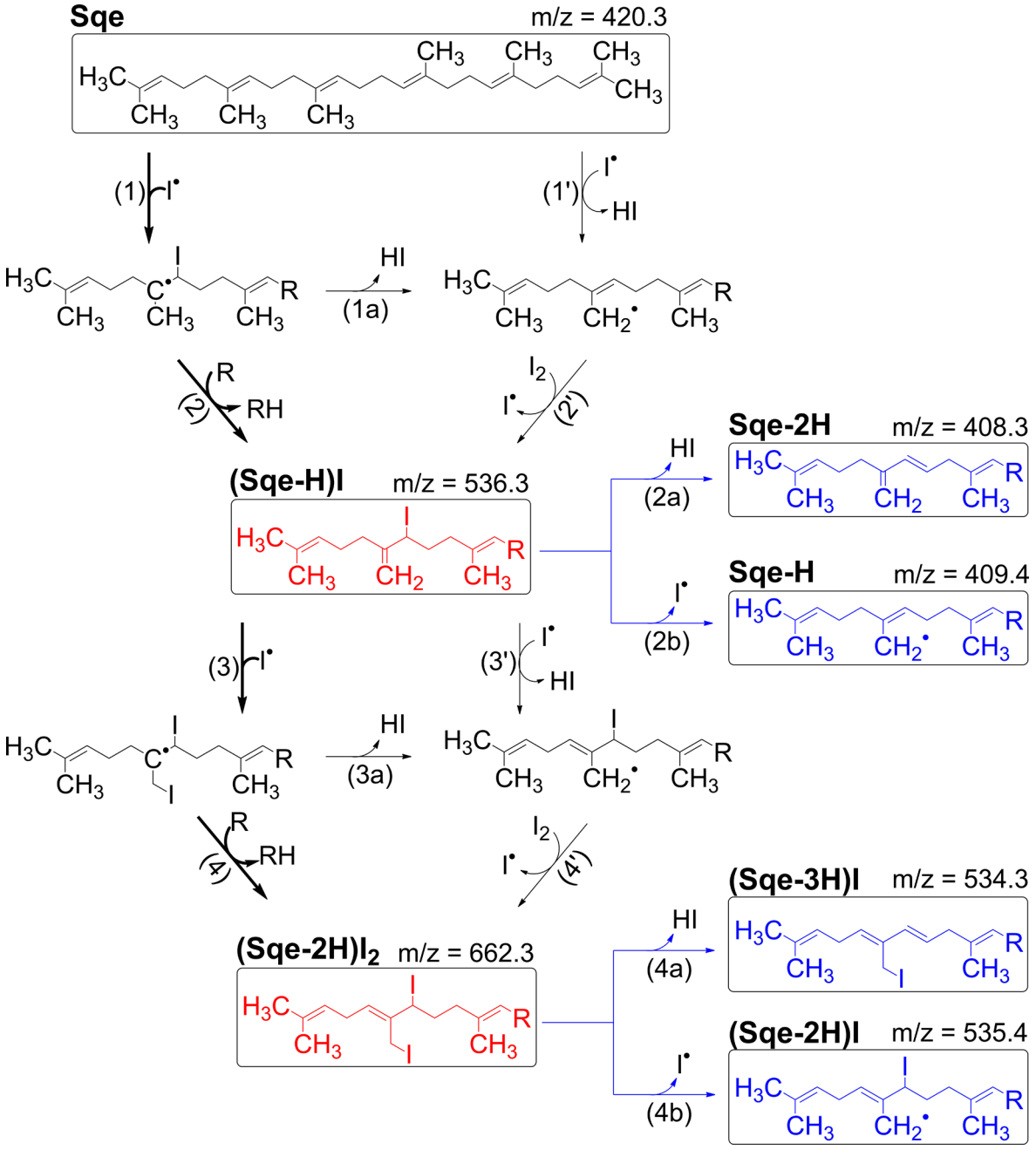

Figure 6. Proposed mechanism for the reaction of squalene with I atoms. The rounded rectangles indicate products observed in this study. Red colored items ((Sqe-H)I and (Sqe-2H)I_2) are the first and second generation squalene products, while in blue color (Sqe-H, Sqe-2H, (Sqe-2H)I and (Sqe-3H)I) are the products formed as a result of dissociative photoionization of (Sqe-*n*H)I_n products, which result in the elimination of HI or I atom (see text for more details). The bold arrows indicate the reaction path that is expected to have the major contribution to the formation of the detected products. The mechanism as proposed is relevant for any of the squalene C═C double bonds.

atoms. Thus, the peaks observed at m/z = 411, 412, 537, 538, 663, 664 correspond to ^{13}C isotopes of squalene and its iodinated products for singly and doubly ^{13}C substituted molecules. The relative intensities of isotopic peaks are consistent with the carbon chain length given the instrumental uncertainty.

Figure 6 shows a tentative reaction mechanism for the I atom reaction with submicrometer squalene droplets based on reaction products observed in Figure 4. Multiple isomers are expected to be formed for each of the suggested pathways. In addition some of the indicated reactions can occur both at the particle surface as well as within the particle. The initial reactions involve either the addition of an I atom to one of the six squalene double bonds (Figure 6, step 1) to form RI· (SqeI·) or the H atom abstraction by the I atom (Figure 6 step 1′) to form R· (Sqe-H·) alkyl radicals.

Since direct addition of the I atom to a double bond yields a radical species (as already mentioned above, to form SqeI·), it is likely that hydrogen abstraction takes place immediately after, resulting in the formation of the (Sqe-H)I reaction product (Figure 6, step 2). The addition of the I atom to a squalene double bond might also be followed by HI elimination and consequently to form a Sqe-H· radical species (Figure 6, step 1a), in an addition−elimination reaction fashion.

dx.doi.org/10.1021/jp5085247 | J. Phys. Chem. A 2014, 118, 10688−10698

The SqeI· alkyl radical might also gain a hydrogen atom from an adjacent hydrocarbon molecule and could form SqeHI. Previous studies by Lee et al.[19] on NO_3 oxidation of squalene particles showed that a H atom is abstracted from an adjacent squalene molecule by the nitroalkyl radical, which is formed by the initial NO_3 addition to the C=C double bond of the squalene particle. However, on the basis of the signal-to-noise ratio of the present experiment, no evidence for the SqeHI product formation is observed. The absence of SqeHI in the product mass spectrum may also be due to its dissociative photoionization to yield HI and a squalene molecule. Since no other products that might originate from SqeHI are present in the recorded mass spectra (as observed by Lee et al.[19]), this path is not considered in the reaction scheme in Figure 6.

As already mentioned above, direct hydrogen atom abstraction by the I atom might also be possible (Figure 6, step 1′). Although the results observed here for squalane particles suggest that the I atom is essentially inert toward saturated bonds, the presence of $C(sp^3)$−H bonds in the squalene structure that are allylic in character and, in consequence, have a significantly lower bond energy makes those bonds more reactive than their equivalent in squalane. The H-abstraction at these bonds is more exothermic and has considerably lower activation energy. Thus, the enthalpies of abstraction from allylic carbons are typically between −56 and −86 kJ·mol^{-1}, while abstraction reactions from saturated hydrocarbons have enthalpy values between −7 and −43 kJ·mol^{-1}, depending on the type of abstracted H.[31] The resulting radical species Sqe-H· further reacts either with an I atom or with an I_2 molecule to form (Sqe-H)I iodinated product (Figure 6, step 2′). Both reaction channels (Figure 6, step 1) and (Figure 6, step 1′) in Figure 6 lead to the formation of (Sqe-H)I via step 2 and step 2′ in Figure 6. However, because of the experimental limitations, we cannot distinguish between the contributions of channels 1 and 1′ (cf. Figure 6) that lead to the observed (Sqe-H)I reaction product. Nevertheless, the H abstraction channel (Figure 6, step 1′) is expected to have a minor contribution to the observed reaction products with respect to the addition channel (Figure 6, step 1).

Dissociative photoionization of (Sqe-H)I leads to the formation of multiple fragment ion peaks (see peaks below mass m/z = 410 in Figure 4c). For instance, the blue colored species in Figure 6 (Sqe-H and Sqe-2H) might correspond to Sqe-H (m/z = 409) and Sqe-2H (m/z = 408) generated via dissociative photoionization of (Sqe-H)I via I and HI loss, respectively. The exact origin of the peaks observed at masses m/z = 407−403 in Figure 4c, left panel, is not fully understood. The peaks corresponding to odd masses, e.g., m/z = 407, 405, 403 are radicals, and therefore, they should be exclusively formed via dissociative photoionization of higher molecular mass species formed in the flow tube during the reaction. The peaks corresponding to even masses might be produced by dissociative photoionization, but they could also be a result of some complex chemical reactions, such as particle phase chemistry as already mentioned above.

A similar scenario as described above for (Sqe-H)I product formation is assumed to be followed in the case of the (Sqe-2H)I_2 product. Iodine atom attack on the first generation product (Sqe-H)I (Figure 6, step 3) followed by hydrogen abstraction would result in the formation of the second iodinated product, (Sqe-2H)I_2, observed in the experiment. A second channel, contributing to the formation of (Sqe-2H)I_2 species, participating in an addition−elimination scenario, might also be possible (Figure 6, steps 3 and 3a). A minor contribution to the formation of (Sqe-2H)I_2 might be via hydrogen atom abstraction from (Sqe-H)I by the I atom followed by reaction either with the I atom or with the I_2 molecule (Figure 6, steps 3′ and 4′).

As mentioned above, peaks corresponding to (Sqe-nH)I (n = 2, 3, 4, 5) are detected in the mass spectrum (Figure 4c, middle panel). These peaks might be attributed to dissociative photoionization of (Sqe-2H)I_2. For example, (Sqe-2H)I and (Sqe-3H)I could be attributed to dissociative photoionization of (Sqe-2H)I_2 (cf. reaction steps 4a and 4b in Figure 6).

Extremely small peaks corresponding to (Sqe-nH)I_2 (n = 3, 4,) are also observed (cf. Figure 4c, left panel). They suggest, considering a similar formation mechanism as discussed above, that (Sqe-3H)I_3 is also potentially formed. However, (Sqe-3H)I_3 is not detected in this experiment, most likely because of the low amount of this product that is formed and the fact that it also subsequently undergoes dissociative photoionization. According to the reaction mechanism proposed in this work, double bonds can be re-formed during the reaction, e.g., species like (Sqe-2H)I_2 in Figure 6, and consequently more than six addition reactions could occur if the reaction sequence reaches completion. The main reaction mechanism that leads to the formation of (Sqe-H)I and (Sqe-2H)I_2 is attributed to the I atom addition mechanism. Therefore, in Figure 6 this path is indicated by bold arrows.

The tentative reaction mechanism proposed in this work can explain the formation of iodinated squalene reaction products as observed in the experiment. However, the mechanism of squalene reaction with the iodine atom might proceed in a more complex manner.

The kinetic evolution of squalene and its first two groups of higher molecular weight iodinated reaction products, (Sqe-H)I and (Sqe-2H)I_2, as a function of iodine atom exposure is shown in Figure 7. In all the results reported here, where kinetics is measured, the I atom exposure is varied by keeping the flow rate, i.e., reaction time, constant and varying the I atom concentration. For comparison, Figure 7a displays the normalized decay of squalene ($[Sqe]/[Sqe]_0$) (black open symbols) and squalane ($[Sq]/[Sq]_0$) (red open symbols) as a function of I exposure. The kinetic evolution of squalene iodinated products is displayed in Figure 7b and Figure 7c. As can be seen in Figure 7b and Figure 7c, both (Sqe-H)I and (Sqe-2H)I_2 iodinated products exhibit a complex dependence on the I atom exposure. Each product is formed followed by a decay at higher I exposures in the case of (Sqe-H)I (see Figure 7b). The (Sqe-2H)I_2 signal is observed to reach a plateau at higher I exposure (see Figure 7c).

3.3. Effective Uptake Coefficient. The normalized decays of squalane ($[Sq]/[Sq]_0$) and squalene ($[Sqe]/[Sqe]_0$) as a function of I exposure (Figure 7a) are further used to determine the effective reactive uptake coefficients.

Upon the basis of the estimated sensitivity of the experimental setup, we derive an upper limit for squalane reactive uptake coefficient. Thus, the normalized squalane signal ($[Sq]/[Sq]_0$) plotted versus $\langle I\rangle_t t$ (red circles in Figure 7a) is fitted to a single exponential decay function (red solid line in Figure 7a) to determine k_{Sq}. The effective uptake coefficient is subsequently computed using eq 1, and an upper limit for $\gamma_I^{Sq} \leq 8.58 \times 10^{-7}$ is determined.

The decay constant, $k_{Sqe} = (1.65 \pm 0.71) \times 10^{-16}$ cm^3·s^{-1}·molecule^{-1} with the I atom exposure, is obtained from a single exponential decay fit to the squalene trace (black solid line in

dx.doi.org/10.1021/jp5085247 | J. Phys. Chem. A 2014, 118, 10688−10698

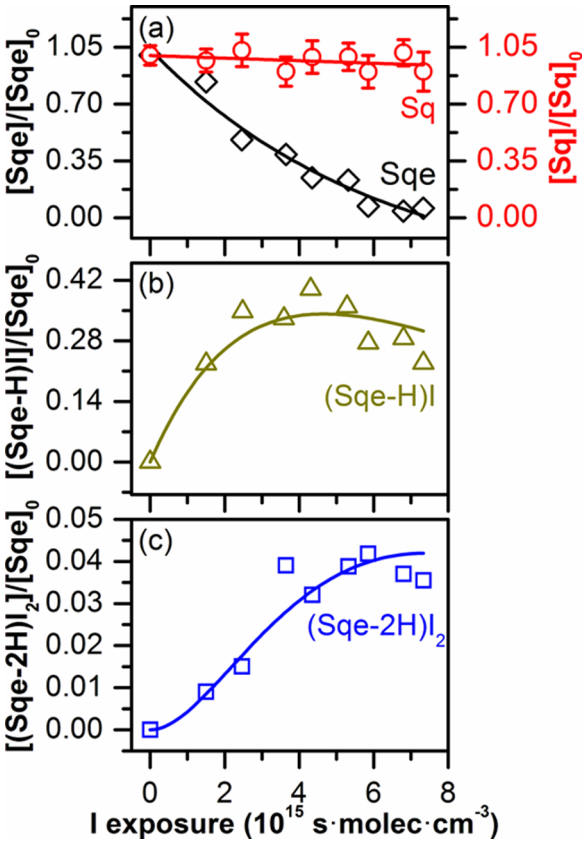

Figure 7. Kinetic evolution of (a) squalane (open red circles), squalene (open black diamond), and (b, c) squalene first two iodinated products ((Sqe-H)I and (Sqe-H_2)I_2) measured as a function of iodide exposure. The symbols correspond to the measured data, while the solid lines in panel a correspond to a fit using single exponential function. The solid lines in panels b and c represent the fit to the experimental data assuming that the (Sqe-H)I and (Sqe-H_2)I_2 reaction products are formed with equal probability; see text for more details.

Figure 7a). The effective uptake coefficient is then computed using the same eq 1. A value of $\gamma_I^{Sqe} = (1.20 \pm 0.52) \times 10^{-4}$ for the squalene reactive uptake coefficient is obtained at an average I concentration of 1.5×10^{14} molecules·cm^{-3}.

An additional source of error is due to the error from the determination of the I atom absolute concentration. In order to see how the effective uptake coefficient explicitly depends on the absolute I atom concentration, the value of the reactive uptake coefficient was calculated for two extreme cases. The concentration of I atoms in the flow tube is assumed to be 5 times lower or 5 times higher than obtained using the Kinetica2003 software. The obtained effective uptake coefficients are $(6.20 \pm 2.66) \times 10^{-4}$ and $(2.50 \pm 1.07) \times 10^{-5}$, respectively. As expected, the value of the reactive uptake coefficient changes by assuming different I atom concentrations in the flow tube reactor (5 times less and 5 times more than the I atom concentration calculated using Kinetica2003 software), but even in these extreme cases the values for the effective uptake coefficient are still very small, corresponding to a very slow reaction.

The kinetic evolution of (Sqe-H)I and (Sqe-2H)I_2 reaction products displayed in Figure 7b and Figure 7c are fit using eq 5 to approximate the rates of formation of these products.[21] Equation 5 describes a sequential oxidation mechanism in a particle that is well mixed on the time scale of the reaction.

$$\frac{[(\text{Sqe-}n\text{H})\text{I}_n]}{[\text{Sqe}]_0} = B_n \frac{(k \cdot \langle \text{I} \rangle_t \cdot t)^n}{n!} \exp(-k \cdot \langle \text{I} \rangle_t \cdot t) \quad (5)$$

In eq 5 k represents the second order heterogeneous rate constant while n denotes the product generation. In the case of unreacted squalene $n = 0$. B_n is an adjustable parameter to account for differences in isotope abundance, VUV photoionization efficiency, and fragmentation patterns of the oxidation products and squalene. For simplicity, k in eq 5 is fixed to the value obtained from the exponential fit of the squalene decay curve shown in Figure 7a. The kinetic evolution of the squalene products ((Sqe-H)I and (Sqe-2H)I_2) is then modeled to fit the data, using eq 5, by exclusively adjusting the B_n parameter, with n characterizing the iodination generation. Model fits to the (Sqe-H)I and (Sqe-2H)I_2 experimental data are displayed in Figure 7b and Figure 7c as solid lines. Within the experimental error, the overall kinetic evolution of the parent compound and its first two generations of reaction products can be reasonably fit using a single rate constant. This indicates that for the squalene + I reaction $\gamma_I^{Sqe} = (1.20 \pm 0.52) \times 10^{-4} \approx \gamma_I^{(Sqe\text{-}H)I} \approx \gamma_I^{(Sqe\text{-}2H)I_2}$. However, as double bonds are consumed, the reactive collision probability will decrease.

The calculated value of the effective uptake coefficient ($\gamma_I^{Sqe} = (1.20 \pm 0.52) \times 10^{-4}$) indicates that on average only one squalene molecule is reacted in a particle per 10 000 collisions between I atoms and the squalene particles. Therefore, I atoms might diffuse within the particle instead of directly reacting with or scattering from the particle surface. Slow diffusion into the particle and fast reactive loss would suggest that reactions occur close to the gas−surface interface, whereas fast diffusion and slow reactions would result in reactions throughout the bulk of a particle.[32] The value of reacto-diffusive length (l_{RD}) might give some indication about the nature of this reaction. l_{RD} represents the typical distance an atom or a molecule will diffuse before reacting, and it is consequently a measure of the concentration gradient of the reactant in the aerosol:[33,34]

$$l_{RD} = \sqrt{\frac{D_P}{k^I}} \quad (6)$$

where D_P ($cm^2 \cdot s^{-1}$) represents the diffusion coefficient of the I atom in the particle, k^I (s^{-1}) is the pseudo-first-order rate constant for reaction of I in the particle, and $k^I = k^{II}[\text{Sqe}]$. k^{II} is the second-order heterogeneous rate constant for the reaction of an I atom and squalene particle and is here equal to k_{Sqe}. D_P is estimated to be 10^{-5} $cm^2 \cdot s^{-1}$.[32] By use of eq 6, the reacto-diffusive length is then estimated to be ~69 nm, which suggests that I atoms might significantly diffuse inside the particle prior to reaction. However, this value is just an estimate, since it does not take into account the loss of I atoms, possibly by recombination on the surface of the droplet or inside the droplet, which competes with the I atom addition to the double bond of squalene.

For comparison we calculate the reacto-diffusive length in the case of Cl atoms with squalane particles in the presence of 20% O_2, with O_2 acting as scavenger for particle-phase secondary chain chemistry propagation. This is known as a very reactive system and has a much larger value of the reactive uptake coefficient ($\gamma_{Cl}^{Sq} = 0.65 \pm 0.07$) than the one measured in the case of the I + squalene reaction.[18] By use of the same procedure as described above to calculate the reacto-diffusive

dx.doi.org/10.1021/jp5085247 | J. Phys. Chem. A 2014, 118, 10688−10698

length, a value of $l_{DR} \approx 0.66$ nm is estimated for the Cl + squalane reaction in the oxygen presence. This length is on the order of a few particle layers and is consistent with the reaction occurring very close to the surface of the particle rather than inside the particle. Unlike more reactive systems where the reaction occurs in a near surface layer, we would expect that I atoms may diffuse significantly into the particle before reacting because the reacto-diffusive length is near the value of the particle radius.

The gas-phase reaction between different alkenes and I atoms has been investigated for a variety of reaction temperatures by a number of groups.[14,15,35] No iodinated product formation has been observed for temperatures slightly above ambient temperature. In addition, the presence of catalytic amounts of I atom, in the alkenes + I atom reaction, results in a positional (hydrogen shift) as well as geometrical (cis−trans) isomerization of the investigated alkenes.

Compared to the gas phase reactions, there are potentially more highly coupled reactions taking place between reactants, products, and intermediates in the case of heterogeneous reactions. As a consequence, reactions that normally do not take place in the gas phase are found to have an enhanced surface reaction probability. Various studies revealed that the surface reactions induced by small radicals or atoms can be enhanced by several orders of magnitude over analogous bimolecular reactions in the gas phase. Moise et al.[6] measured large surface enhancement factors for gas phase reactions that are slow ($k < 10^{-15}$ cm^3·molecule^{-1}·s^{-1}) because of high activation energies, in contrast with fast reactions ($k < 10^{-12}$ cm^3·molecule^{-1}·s^{-1}), which exhibit minimal surface enhancement. The exact mechanism for this reaction enhancement remains currently ambiguous but may originate, in part, from multiple scattering or trapping of reactant species at the interface, thus increasing the overall chance of a reactive encounter.[36−38] Furthermore, Wandia et al. also observed an enhancement in the case of ozone reaction with a phospholipid film compared to a typical gas phase ozone−alkene reactions.[39] Their results in conjunction with molecular dynamics simulation suggest that the observed enhanced reactivity compared to the one in the gas phase may be due to trapping of ozone in the porous hydrocarbon layer, which increases the probability of an encounter of O_3 with a double bond.

On the basis of the calculated value of reacto-diffusive length of iodine into squalene particles, which has a value comparable to the squalene particle radius, it is likely that the observed reaction between squalene submicrometer droplets and I atoms is due to the long time trapping of reactive I atoms in the particle, which considerably increases the probability of an encounter of the I atom with a C=C double bond. The trapping and consequently the multiple interactions of the reagents, i.e., 10 000 collisions or more, in the aerosol particles are the key to why iodinated hydrocarbons are formed at room temperature just in the aerosol particle and not in the gas phase.

4. CONCLUSION

The present investigations reveal new insights into a category of reactions with low probability in the gas phase but that present an enhanced probability in the heterogeneous phase. The reactions of I atoms with submicrometer squalane and squalene droplets were investigated here by monitoring the heterogeneous reaction, using VUV photoionization aerosol mass spectrometry. While the unsaturated squalane particles appear to be unreactive toward I atoms under our experimental conditions, the saturated squalene particles slowly react with I atoms and iodinated hydrocarbon molecules are formed and detected. Despite the fact that similar gas-phase reactions are expected to have extremely low probability, the reaction of I atoms with squalene particles takes on a probability of 10^{-4} due to the trapping and consequently the multiple interactions of the I atoms into the squalene aerosol particles. The effective reactive uptake coefficient and the distribution of the iodinated products are measured. Within experimental error, the chemical evolution of squalene and its iodinated products can all be represented by a single kinetic rate parameter. The effective uptake coefficient measured for unsaturated hydrocarbon squalene is found to be about 3 orders of magnitude larger than the one estimated for saturated hydrocarbon squalane.

AUTHOR INFORMATION

Corresponding Author

*E-mail: srl@berkeley.edu. Phone: (+1) 510-643-5467. Fax: (+1) 510-643-1367.

Notes

The authors declare no competing financial interest.

ACKNOWLEDGMENTS

This work was supported by the Director, Office of Energy Research, Office of Basic Energy Sciences, Chemical Sciences Division of the U.S. Department of Energy under Contract DE-AC02-05CH11231. The authors acknowledge constructive discussions with Dr. M. D. Ward and the technical assistance from Dr. D. J. Taube. In particular, D.M.P.-V. is grateful to the Alexander von Humboldt Foundation for a Feodor Lynen fellowship.

REFERENCES

(1) Lazár, M.; Rychly, J.; Klimo, V.; Pelikán, P.; Valko, L. *Free Radicals in Chemistry and Biology*; CRC Press: Boca Raton, FL, 1989.
(2) Chatgilialoglu, C.; Studer, A. *Encyclopedia of Radicals in Chemistry, Biology and Materials*; Wiley: Chichester, U.K., 2012.
(3) Finlayson-Pitts, B. J.; Pitts, J. N. *Atmospheric Chemistry*; Wiley: New York, 1986.
(4) Wayne, R. P. *Chemistry of Atmospheres*; Clarendon: Oxford, U.K., 1985.
(5) Warnatz, J. *Combustion Chemistry*; Springer-Verlag: New York, 1984.
(6) Moise, T.; Rudich, Y. Uptake of Cl and Br by Organic Surfaces—A Perspective on Organic Aerosols Processing by Tropospheric Oxidants. *Geophys. Res. Lett.* **2001**, *28*, 4083−4086.
(7) Calvert, J. G.; Pitts, J. N. *Photochemistry*; Wiley: New York, 1966.
(8) Tellinghuisen, J. Resolution of the Visible-Infrared Absorption Spectrum of I_2 into Three Contributing Transitions. *J. Chem. Phys.* **1973**, *58*, 2821−2834.
(9) Ouchi, M.; Terashima, T.; Sawamoto, M. Transition Metal-Catalyzed Living Radical Polymerization: Toward Perfection in Catalysis and Precision Polymer Synthesis. *Chem. Rev.* **2009**, *109*, 4963−5050.
(10) Teranishi, H.; Benson, S. W. The Kinetics of Dehydrogenation of Isobutane by Iodine and the Heat of Formation of the *t*-Butyl Radical. *J. Am. Chem. Soc.* **1963**, *85*, 2887−2890.
(11) Goy, C. A.; Pritchard, H. O. Kinetics and Thermodynamics of the Reaction between Iodine and Methane and the Heat of Formation of Methyl Iodide. *J. Phys. Chem.* **1965**, *69*, 3040−3042.
(12) Knox, J. H.; Musgrave, R. G. Iodination of Alkanes: Ethane, Propane and Isobutane. *Trans. Faraday Soc.* **1967**, *63*, 2201−2216.
(13) Golden, D. M.; Walsh, R.; Benson, S. W. The Thermochemistry of the Gas Phase Equilibrium $I_2 + CH_4 \rightleftarrows CH_3 + HI$ and the Heat of

Formation of the Methyl Radical. *J. Am. Chem. Soc.* **1965**, *87*, 4053−4057.
(14) Back, M. H.; Cvetanović, R. J. Reactions of Iodine Atoms with *n*-Butenes. I. Cis−Trans Isomerization of Butene-2. *Can. J. Chem.* **1963**, *41*, 1396−1405.
(15) Back, M. H.; Cvetanović, R. J. Reactions of Iodine Atoms with *n*-Butenes: II. Interconversion of Butene-1 and Butene-2. *Can. J. Chem.* **1963**, *41*, 1406−1413.
(16) Hepperle, S. S.; Li, Q.; East, A. L. L. Mechanism of Cis/Trans Equilibration of Alkenes via Iodine Catalysis. *J. Phys. Chem. A* **2005**, *109*, 10975−10981.
(17) Benson, S. W.; Egger, K. W.; Golden, D. M. Iodine-Catalyzed Isomerization of Olefins. III. Kinetics of the Geometrical Isomerization of Butene-2 and the Rate of Rotation about a Single Bond. *J. Am. Chem. Soc.* **1965**, *87*, 468−476.
(18) Liu, C.-H.; Smith, J. D.; Che, D. L.; Ahmed, M.; Leone, S. R.; Wilson, K. R. The Direct Observation of Secondary Radical Chain Chemistry in the Heterogeneous Reaction of Chlorine Atoms with Submicron Squalane Droplets. *Phys. Chem. Chem. Phys.* **2011**, *13*, 8993−9007.
(19) Lee, L.; Wooldridge, P.; Nah, T.; Wilson, K.; Cohen, R. Observation of Rates and Products in the Reaction of NO_3 with Submicron Squalane and Squalene aerosol. *Phys. Chem. Chem. Phys.* **2013**, *15*, 882−892.
(20) Nah, T.; Kessler, S. H.; Daumit, K. E.; Kroll, J. H.; Leone, S. R.; Wilson, K. R. Influence of Molecular Structure and Chemical Functionality on the Heterogeneous OH-Initiated Oxidation of Unsaturated Organic Particles. *J. Phys. Chem. A* **2014**, *118*, 4106−4119.
(21) Smith, J. D.; Kroll, J. H.; Cappa, C. D.; Che, D. L.; Liu, C. L.; Ahmed, M.; Leone, S. R.; Worsnop, D. R.; Wilson, K. R. The Heterogeneous Reaction of Hydroxyl Radicals with Sub-Micron Squalane Particles: A Model System for Understanding the Oxidative Aging of Ambient Aerosols. *Atmos. Chem. Phys.* **2009**, *9*, 3209−3222.
(22) Gloaguen, E.; Mysak, E. R.; Leone, S. R.; Ahmed, M.; Wilson, K. R. Investigating the Chemical Composition of Mixed Organic-Inorganic Particles by "Soft" Vacuum Ultraviolet Photoionization: The Reaction of Ozone with Anthracene on Sodium Chloride Particles. *Int. J. Mass. Spectrom.* **2006**, *258*, 74−85.
(23) Liu, P.; Ziemann, P. J.; Kittelson, D. B.; McMurry, P. H. Generating Particle Beams of Controlled Dimensions and Divergence: I. Theory of Particle Motion in Aerodynamic Lenses and Nozzle Expansions. *Aerosol Sci. Technol.* **1995**, *22*, 293−331.
(24) Liu, P.; Ziemann, P. J.; Kittelson, D. B.; McMurry, P. H. Generating Particle Beams of Controlled Dimensions and Divergence: II. Experimental Evaluation of Particle Motion in Aerodynamic Lenses and Nozzle Expansions. *Aerosol Sci. Technol.* **1995**, *22*, 314−324.
(25) Richardson, D. E. *Kinetica2003*; Department of Chemistry, University of Florida: Gainesville, FL, 2003; http://www.chem.ufl.edu/~der/Kinetica2003.htm.
(26) Jenkin, M. E.; Cox, R. A.; Mellouki, A.; Bras, G. L.; Poulet, G. Kinetics of the Reaction of Iodine Atoms with Hydroperoxy Radicals. *J. Phys. Chem.* **1990**, *94*, 2927−2934.
(27) Capelle, G. A.; Broida, H. P. Lifetimes and Quenching Cross Sections of $I_2(B^3\Pi_{Ou}^+)$. *J. Chem. Phys.* **1973**, *58*, 4212−4222.
(28) Kireev, S. V.; Shnyrev, S. L. Collisional Predissociation of Vibrational Levels of the *B* State in I_2 Excited by 633-nm Radiation of a He−Ne Laser. *Laser Phys.* **1998**, *8*, 483−486.
(29) Rabinowitch, E.; Wood, W. C. Dissociation of Excited Iodine Molecules. *J. Chem. Phys.* **1936**, *4*, 358−362.
(30) Saiz-Lopez, A.; Saunders, R. W.; Joseph, D. M.; Ashworth, S. H.; Plane, J. M. C. Absolute Absorption Cross-Section and Photolysis Rate of I_2. *Atmos. Chem. Phys.* **2004**, *4*, 1443−1450.
(31) Lide, D. R. *Handbook of Chemistry and Physics 2004−2005: A Ready-Reference Book of Chemical and Physical Data*; CRC Press: Boca Raton, FL, 2004.
(32) Abbatt, J. P. D.; Lee, A. K. Y.; Thornton, J. A. Quantifying Trace Gas Uptake to Tropospheric Aerosol: Recent Advances and Remaining Challenges. *Chem. Soc. Rev.* **2012**, *41*, 6555−6581.
(33) Schwartz, S. E.; Freiberg, J. E. Mass-Transport Limitation to the Rate of Reaction of Gases in Liquid Droplets: Application to Oxidation of SO_2 in Aqueous Solutions. *Atmos. Environ.* **1981**, *15*, 1129−1144.
(34) Hanson, D. R.; Ravishankara, A. R.; Solomon, S. Heterogeneous Reactions in Sulfuric Acid Aerosols: A Framework for Model Calculations. *J. Geophys. Res.* **1994**, *99*, 3615−3629.
(35) Golden, D. M.; Egger, K. W.; Benson, S. W. Iodine-Catalyzed Isomerization of Olefins. I. Thermodynamic Data from Equilibrium Studies of Positional and Geometrical Isomerization of 1-Butene and 2-Butene. *J. Am. Chem. Soc.* **1964**, *86*, 5416−5420.
(36) Garton, D. J.; Minton, T. K.; Alagia, M.; Balucani, N.; Casavecchia, P.; Volpi, G. G. Comparative Dynamics of $Cl(^2P)$ and $O(^3P)$ Interactions with a Hydrocarbon Surface. *J. Chem. Phys.* **2000**, *112*, 5975−5984.
(37) Nathanson, G. M. Molecular Beam Studies of Gas−Liquid Interfaces. *Annu. Rev. Phys. Chem.* **2004**, *55*, 231−255.
(38) Bagot, P. A. J.; Waring, C.; Costen, M. A.; McKendrick, K. G. Dynamics of Inelastic Scattering of OH Radicals from Reactive and Inert Liquid Surfaces. *J. Phys. Chem. C* **2008**, *112*, 10868−10877.
(39) Wadia, Y.; Tobias, D. J.; Stafford, R.; Finlayson-Pitts, B. J. Real-Time Monitoring of the Kinetics and Gas-Phase Products of the Reaction of Ozone with an Unsaturated Phospholipid at the Air−Water Interface. *Langmuir* **2000**, *16*, 9321−9330.